energies

MDPI

Article

Performance Analysis of Internal Ballistic Multiphase Flow of Composite Charge Structure

Shenshen Cheng *, Kun Jiang *, Shao Xue, Ruyi Tao and Xinggan Lu

School of Energy and Power Engineering, Nanjing University of Science and Technology, Nanjing 210094, China
* Correspondence: css_njust@163.com (S.C.); jkeddy@163.com (K.J.)

Abstract: Different charge structures have different interior ballistic performance. Existing research is based on experimental measurements or the lumped parameter method to obtain limited ballistic characteristics, which indirectly impacts the analysis of the parameters' distribution, requiring a complex modeling solution process. Besides this, the ignition performance of different charge structures needs to be further explored. The disadvantages of previous studies have limited the feasibility of further optimization of the composite charge structure. In this paper, we apply a two-dimensional two-phase flow method based on the Eulerian–Lagrangian model to study the performance of different composite charge structures. First, we establish the mathematical model of different particle types based on interior ballistics, which is directly related to the research foundation of subsequent ballistic performance. Next, we investigate the multi-scale reaction flow of complex charge structures by the two-phase flow method and obtain the distribution of parameters in the chamber. Finally, we conduct a study with different particle charge parameters to explore the sensitivity of ballistic characteristics to structural parameters. The results show that the tubular propellant has good ignition performance in different charge structures, and the ignition consistency can be improved by charging tubular propellant in the center of the chamber. However, more tubular propellants are ineffective at significantly improving ignition performance, and result in a decrease in combustion chamber pressure. These results may be promising for the optimization of various charge structures.

Keywords: charge structure; two-phase flow; numerical simulation; interior ballistic

Citation: Cheng, S.; Jiang, K.; Xue, S.; Tao, R.; Lu, X. Performance Analysis of Internal Ballistic Multiphase Flow of Composite Charge Structure. *Energies* **2023**, *16*, 2127. https://doi.org/10.3390/en16052127

Academic Editors: Zheyan Jin, Zhiwen Gan and Haiyang Hu

Received: 30 November 2022
Revised: 26 December 2022
Accepted: 28 December 2022
Published: 22 February 2023

1. Introduction

The performance of the propulsion system can be improved by adjusting the charge structure. The regularity of the ignition, flame spreading, and propellant combustion are directly affected by the charge structure [1–3]. In order to meet ballistic, tactical, production and economic requirements, the charge structure needs to be adapted to different propulsion system types and propellant types.

The characteristics of large-caliber artillery are a large charging mass and long chamber; therefore, in order to ensure the ignition consistency, most use tubular propellant [4–6]. Compared with granular propellant, the combustion surface of tubular propellant is small, which is not conducive to the formation of high chamber pressure and high muzzle velocity, and the degree of mechanization and automation is low [7–10]. In contrast, in medium-caliber artillery, the composite charge structure is composed of tubular propellant with good ignition performance and granular propellant with good combustion performance [11,12,12]. This not only avoids the hidden danger caused by the high density of single granular propellant, but also avoids the shortcoming of a single tubular propellant being unable to meet the requirements of combat technical indicators. In addition, for the fin-stabilized projectile, some small granular propellant should be inserted into the tail to ensure the charging density in the chamber [13–15]. Consequently, to obtain good interior ballistic performance for different artillery types, complex charge structures will be formed in the chamber.

Meanwhile, the different particle sizes of complex charge structures result in differing ballistic performance. In order to investigate the influence of charge factors on the ballistic performance of composite charge, the multi-scale reaction flow of composite charge structure was numerically simulated. In this way, the combustion characteristics of multi-phase and multi-scale reactive flow of composite charge structure are simulated and revealed theoretically, and the best interior ballistic performance would be obtained. At present, more precise mathematical models and numerical methods are explored in the artillery multi-phase flow theory [16–18]. Recent advances in numerical methods include the application of WENO, AUSM, SHUS and other high-precision schemes, which improve the accuracy of numerical simulation [19–24]. It is easy to realize numerical modeling and calculation while ensuring high precision, and these display good adaptability with different calculation models. Therefore, the application of high-order numerical schemes has become prevalent in the development of internal ballistic two-phase flow.

The main development in mathematical modeling is different particle description methods based on Eulerian–Lagrangian model, such as the particle swarm model of the LPI method and the CFD-DEM model [25–28]. The most essential variation between different methods lies in their different spatial scales. Different methods have different solving accuracy and computational efficiency, so they are suitable for different gas-solid two-phase flow problems. In complex charge structures, different equations of motion need to be established for different types of particle, so the two-fluid method is no longer applicable.

In this paper, the multi-scale, multi-phase flow process in the chamber is normalized by use of the proposed particle element method. The multi-dimensional characteristics of combustion gas and propellant particles in complex charge structures are simulated in detail, and the ballistics performance and flow field distribution of different charge structures are discussed. Ultimately, the sensitivity of gun interior ballistic performance to structural parameters is explored by adjusting the charge parameters of different charge structures. The research results can be used to improve the design and performance of various artillery charge structures.

In summary, the main contributions of this study are threefold:

(1) The multi-scale reactive flows of complex charge structures are numerically studied;
(2) The ballistic properties and flow field distribution of different charge structures are discussed in detail; and
(3) The sensitivity of ballistic characteristics to structural parameters is studied by adjusting the charge structure.

2. Mathematical Model

2.1. Governing Equation of Gas Phase

The Eulerian–Lagrangian model, used for the modeling of the interior ballistics, is based on the unsteady reactive two-phase flow with the propellants and their combustion gases [29]. The gas phase applies the Eulerian coordinates, while the solid phase utilizes the Lagrangian coordinates. The gas phase governing equations contain continuity equation, momentum equation, energy equation, and the particle movement equation. Thus, the governing equations are as follows [30]:

$$\frac{\partial(\varphi\rho_g)}{\partial t} + \nabla\cdot(\varphi\rho_g u_g) = \dot{m}_c + \dot{m}_{g,ign} \tag{1}$$

$$\frac{\partial(\varphi\rho_g u_g)}{\partial t} + \nabla\cdot(\varphi\rho_g u_g\cdot u_g) + \varphi\nabla p = -f_s + \dot{m}_c u_p + \dot{m}_{g,ign} u_{g,ign} \tag{2}$$

$$\begin{aligned}&\tfrac{\partial[\varphi\rho_g(e_g+u_g\cdot u_g/2)]}{\partial t} + \nabla\cdot[\varphi\rho_g u_g(e_g + p/\rho_g + u_g\cdot u_g/2)] + p\tfrac{\partial\varphi}{\partial t}\\ &= -Q_p - f_s\cdot u_p + \dot{m}_c H_c + \dot{m}_{g,ign} H_{g,ign}\end{aligned} \tag{3}$$

In the above equations, φ is the volume fraction of gas phase, ρ_g is the gas density, u_g is the gas velocity, e_g is the internal energy of gas phase, p is the pressure of the gas, m_{ign} is the mass flow rate of gas from the igniter, m_c is the mass generation rate of gas due to propellant combustion, f_s is the the interphase drag, u_{ign} is velocity of gas from the igniter, Q_p is the interphase heat transfer, H_c and H_{ign} are the stagnation enthalpy of the gas in the chamber and flow from the igniter.

The governing equation of the particles in the Lagrangian coordinates becomes the velocity equation of the propellants. The equation includes the interphase drag, contact, lift, and gravity forces. Contact, lift, and gravity forces are negligible because they only slightly affect propellant motion [31]. Based on the empirical equation by Ergun, the propellant velocity equation used to calculate the drag force is given as follows:

$$\frac{du_p}{dt} = \frac{1}{\rho_p}\left\{150\frac{\mu_f(1-\alpha)}{\alpha d_p^2} + 1.75\frac{\rho|u_g - u_p|}{d_p}\right\} \times (u_g - u_p) \tag{4}$$

Considering the pressure differential force and interphase resistance, the equation of motion of the tubular propellant can be obtained:

$$\frac{du_p}{dt} = \frac{\oint f_s dx + A_p \Delta p - \dot{m}_c u_p}{m_p} \tag{5}$$

where m_p is the tubular propellant mass, A_p is the tubular propellant area of the axial direction, Δp is the differential pressure at the left and right ends.

2.2. Auxiliary Equation

In order to close the above calculation equations of the gas phase and particle elements, a series of other auxiliary equations need to be provided as follows:

(1) Equation of state of gas phase

The Nobel–Abel equation is used for the equation of state:

$$p\left(\frac{1}{\rho_g} - \alpha\right) = RT_g \tag{6}$$

where R is the specific gas constant and T_g is the gas temperature. The co-volume α compensates for the finite volume occupied by the gas molecules.

(2) Propellant combustion equation

When the solid propellant surface temperature reaches the assumed ignition temperature, the particle starts burning. An empirical burning law is used in the associated burning rate calculations. The production rate of gases per particle is shown as follows:

$$m_c = \frac{(1-\varphi)\rho_p}{1-\psi} \cdot \frac{d\psi}{dt} \tag{7}$$

where ρ_p is the density of solid particles, and ψ is the relative burned percentage of particles. For porous propellant, mass produced by solid propellant combustion is calculated by the geometrical functions of relative burnt percentage [32]:

$$\psi = \begin{cases} \chi Z(1 + \lambda Z + \mu Z^2) & Z \le 1 \\ \chi_s Z(1 - \lambda_s Z) & 1 < Z \le Z_k \\ 1 & Z > Z_k \end{cases} \tag{8}$$

$$\frac{dZ}{dt} = \begin{cases} u_1 p^n / e_1 & Z \le Z_k \\ 0 & Z > Z_k \end{cases} \tag{9}$$

where Z is the relative burnt thickness, Z_k is the relative burnt thickness when porous propellant splits, u_1 and n represent the burning rate coefficient and burning rate index, χ, λ, χ_s, λ_s and μ are shape characteristic parameters of a propellant particle.

The tubular charge bundle burns according to the geometrical combustion law, and the combustion rate equation adopts the exponential formula [33]:

$$\begin{aligned} r_e &= r_{e0} - \int \mu_1 p^n dt \\ r_i &= r_{i0} + \int \mu_1 p^n dt \end{aligned} \tag{10}$$

where, $r_{\mathrm{e}0}$ and $r_{\mathrm{i}0}$ are the initial outer diameter and inner diameter of single tubular drug, respectively. r_{e} and r_{i} are the outer diameter and inner diameter of the tubular drug at any time.

The burning mass of the main charge at any time is:

$$m_g = \sum \rho_p \pi c_1 \left[(r_{e0}^2 - r_{i0}^2) - (r_e^2 - r_i^2) \right] N \tag{11}$$

where c_1 is the length of single tubular charge, and N is the number of roots of the tubular charge bundle at the current position.

(3) Inter-phase drag

A model for drag force f_d proposed by Gough [34] is used to calculate the inter-phase drag:

$$f_d = \frac{(1-\varphi)}{d_p} \left| u_g - u_p \right| (u_g - u_p) \rho_g C_f \tag{12}$$

$$C_f = \begin{cases} 1.75 & 0 < \varphi \le \varphi_0 \\ 1.75[((1-\varphi)\varphi_0)/((1-\varphi_0)\varphi)]^{0.45} & \varphi_0 < \varphi \le \varphi_1 \\ 0.3 & \varphi_1 < \varphi \le 1 \end{cases} \tag{13}$$

where d_p is the effective diameter, C_f is empirical coefficient. φ = $[1 + 0.02(1\text{-}\varphi_0)/\varphi_0]^{-1}$, φ_0 is the settling porosity. C_f of tubular drug is as follows:

$$C_f = \begin{cases} 0.17 & \varphi \le 0.6 \\ 0.17 - 1.52^{\frac{\varphi - 0.6}{0.2}} & 0.6 < \varphi \le 0.8 \\ 0.018 & 0.8 < \varphi \le 1 \end{cases} \tag{14}$$

2.3. Numerical Methods

The conservation equations in compatible forms of gas-phase are coupled quasi-linear inhomogeneous hyperbolic partial differential equations (PDEs) with source terms. The third-order TVD-type Runge–Kutta method is used for advancement in the time term and the fifth-order WENO format is adopted for spatial discretization [35]. Meanwhile, the movement equations for the particle elements are also ODEs; therefore, the Runge–Kutta method is also used.

2.4. Initial and Boundary Conditions

For the interior ballistic progress of this work, the initial calculation conditions in the chamber include the initial environmental parameters and the initial charge conditions of the artillery, with experimental data as the source. There is the reflective boundary condition for the wall, the axisymmetric boundary condition for the axis, and the moving boundary condition for the projectile base. Since the WENO format uses multiple base points for calculation, setting three virtual points outside the boundary converts the boundary points into interior points to participate in the calculation; the calculation accuracy of the boundary points is maintained in this way.

3. Results and Discussion

The interior ballistics process of the standard AGARD 132 mm ballistic gun is validated by the calculation. Only the projectile velocity, the maximum pressure at the chamber and bottom are available, so Figure 1 shows the change in these physical quantities over time. The confidence ranges of different simulations of other internal ballistic codes are marked as the interval in Figure 1, indicating that our results are consistent with the expected results.

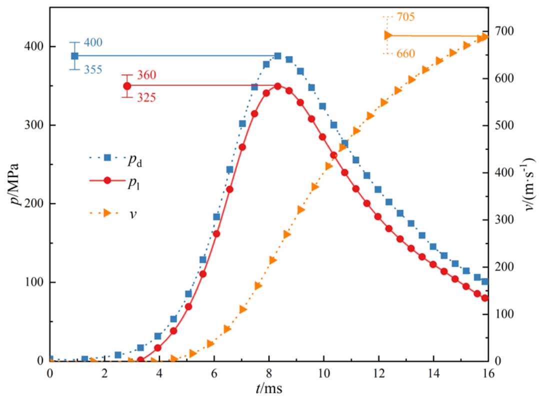

Figure 1. The velocity and pressure over time.

In order to explore the combustion and flow mechanism of different charge structures under real conditions, four typical structures are selected for analysis based on the artillery charging requirements. As shown in Figure 2, under the same chamber structure, four charge cases are charged using tubular propellant and granular propellant, respectively. Case 1 and Case 4 are fully tubular propellants and fully granular propellant charge; Case 2 is the bottom granular propellant charge, suitable for fin-stabilized projectile; and Case 3 is the center tubular propellant charge, suitable for high-density charging. Detailed artillery structure parameters are shown in Table 1, and the charging structure parameters are shown in Table 2.

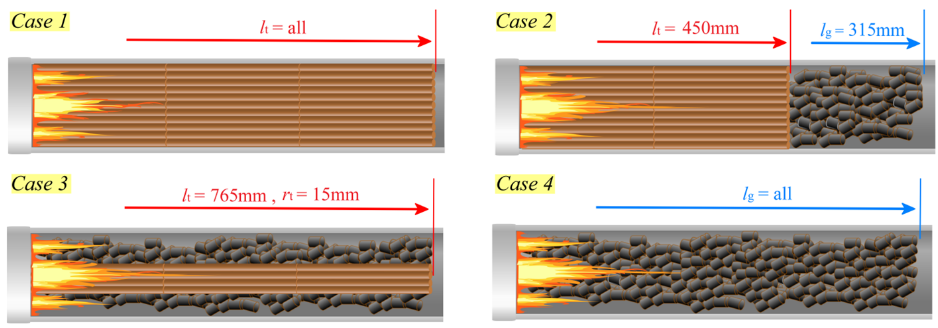

Figure 2. Schematic of different charge structures.

Table 1. The calculation conditions.

Parameters	Value	Parameters	Value
projectile mass/(kg)	45.35	density of powder /(kg/m^3)	1578
calibre/(mm)	132	specific heat ratio	1.27
tubular propellant burn rate coefficient	0.18	granular propellant burn rate coefficient	0.0784
tubular propellant burn rate index	0.75	granular propellant burn rate index	0.9
tubular propellant length (mm)	150	granular propellant length (mm)	25.4
tubular propellant diameter (mm)	6.06	granular propellant diameter (mm)	11.43
tubular propellant perforated diameter (mm)	2.2	granular propellant perforated diameter (mm)	11.43
tubular propellant geometry	7-hole	granular propellant geometry	slotted

Table 2. Charging scheme of different structures.

	Charge Structure	The Mass of Granular/kg	The Mass of Tubular/kg	Charging Density/(g·cm^{-3})
Case 1	fully tubular	9.5	0	0.908
Case 2	bottom granular	5.5	4	0.908
Case 3	center tubular	0.5	9.0	0.908
Case 4	fully granular	0	9.5	0.908

3.1. Ballistic Performance of Different Charge Structures

The four different charge structures are simulated and the pressure curves obtained; these are shown in Figures 3 and 4. As can be seen from the figures, Case 1 has the fastest pressure rise, indicating that its combustion consistency in the chamber is the best. However, the burning surface of tubular propellant is small, resulting in lower gas production rates, so the chamber pressure is minimal. Case 2 was charged with granular propellant charge at the bottom of the bomb compared with Case 1, and the pressure rise was almost the same as Case 1. Due to the presence of granular propellant, the pressure is also slightly higher than Case 1. Therefore, it shows that charging granular propellant at the bottom can effectively ensure the flame transmission performance and improve the chamber pressure.

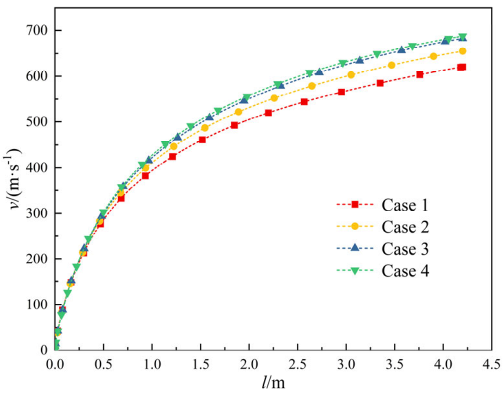

Figure 3. The velocity of the different structures.

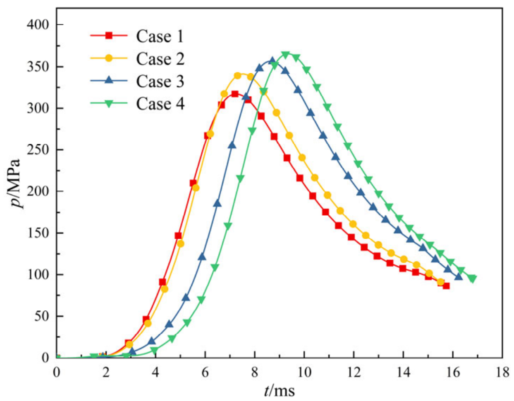

Figure 4. The pressure of the different structures.

Case 4 uses full granular propellant charge, which has poor flame transmission performance and the slowest pressure rise; however, the chamber pressure is highest, due to multiple burning surfaces. Case 3 is charged with tubular propellant in the center of the chamber. As can be seen from the figure, the pressure rises faster than Case 4, and the chamber pressure was only slightly lower than Case 4. This indicates that the central charge structure can guarantee the chamber pressure and improve the ignition consistency.

3.2. Flame Propagation Performance

Figure 5 shows the pressure evolution of different charge structures in the period of ignition transmission. It can be seen from the figure that, in 1.0–2.5 ms, the flame transmission performance of each charge structure is significantly different. In Case 1, the radial effect throughout the chamber disappears quickly. Except for the uneven pressure distribution in the front area during the propagation process, the pressure distribution in other areas is uniform, indicating good flame transmission performance. However, in Case 2, the development of pressure in the area of tubular propellant charge is the same as that of Case 1. There are obvious pressure discontinuities at the boundary of granular propellant and tubular propellant areas; two different pressure distribution areas are formed before and after the discontinuities.

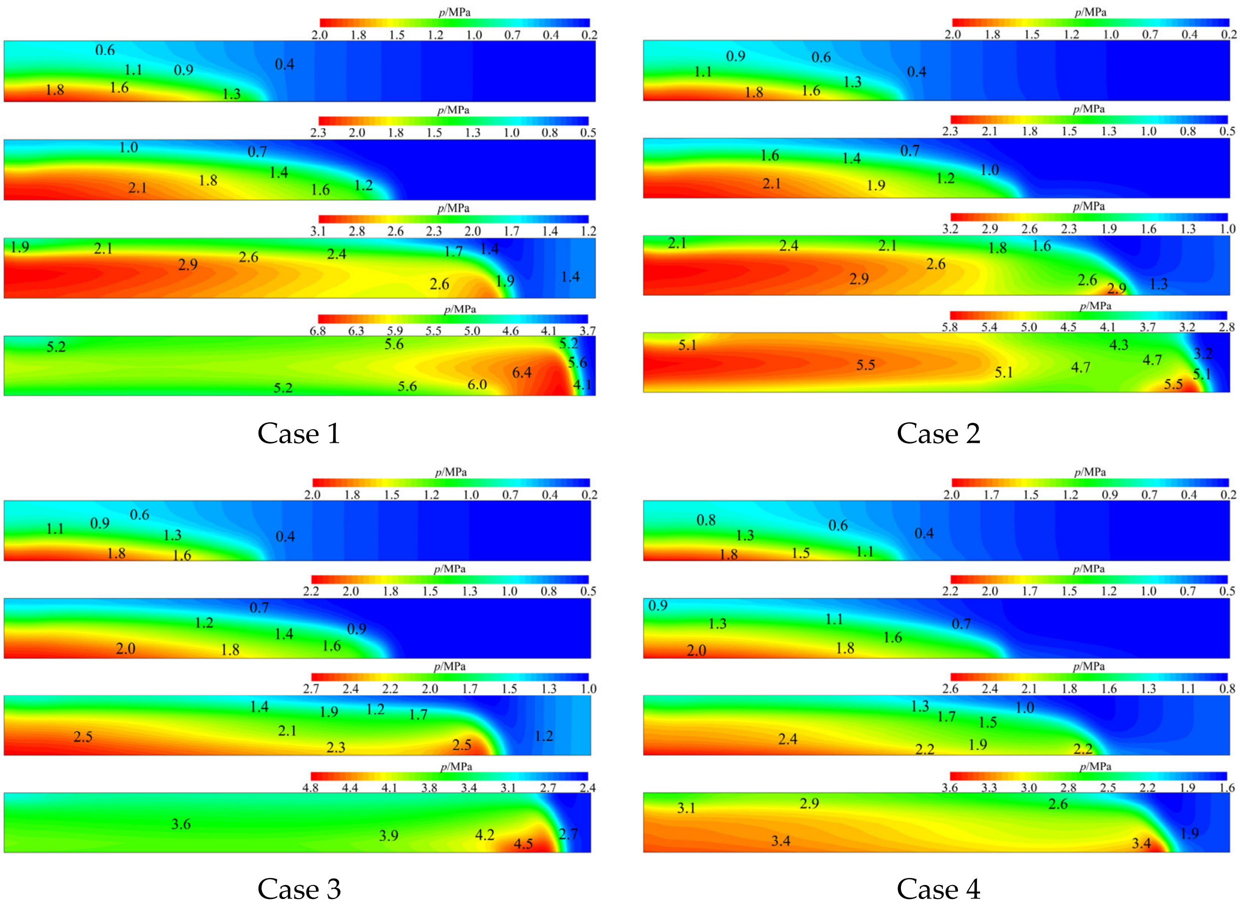

Figure 5. The pressure evolution of different charge structures.

The pressure development law of Case 3 is similar to that of Case 4. In the initial stage, pressure distribution in a radial direction is basically the same. In the axial direction, the bottom pressure of Case 3 rises more quickly, and the pressure distribution in the chamber is more uniform. In contrast, the pressure of Case 4 showed obvious irregular distribution, indicating that the charge structure of Case 3 was more conducive to consistent ignition in the chamber.

Furthermore, the change of ignition time of propellant in the chamber was analyzed. Figure 6 shows the evolution of the ignited area in the chamber of different charge structures at different times. The asterisk represents when this position is ignited, and the different colors indicate the ignition area of the propellant in the chamber at different times. According to the ignition time, the axial flame spreading in the area with tubular propellant is relatively fast, as shown in Case 1 to Case 3. Figure 7 shows the position of axial ignited time, which is significantly higher than the axial transmission of granular propellant.

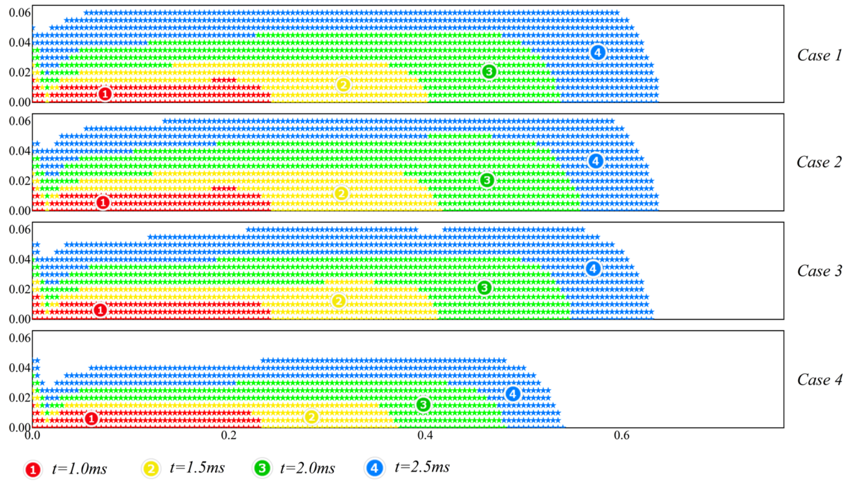

Figure 6. The evolution of the ignited area in the chamber of different charge structures.

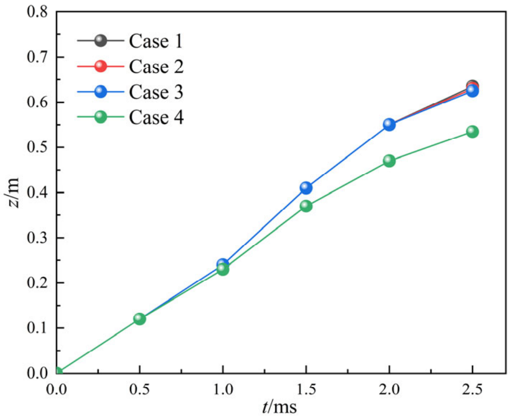

Figure 7. Axial flame transmission.

In terms of radial flame transmission, the charge structure of Case 1 and Case 2 is basically the same, so the law of radial flame transmission in the early stage is close to the same. However, in Case 4, the radial flame transmission of granular propellant was obviously hindered. Radial ignited time is shown in Figure 8. The radial transmission of granular propellant is the worst, and the effect of central charge structure is better than that of granular propellant, because of partial tubular propellant. In general, the ignition consistency of tubular propellant is significantly better than that of granular propellant.

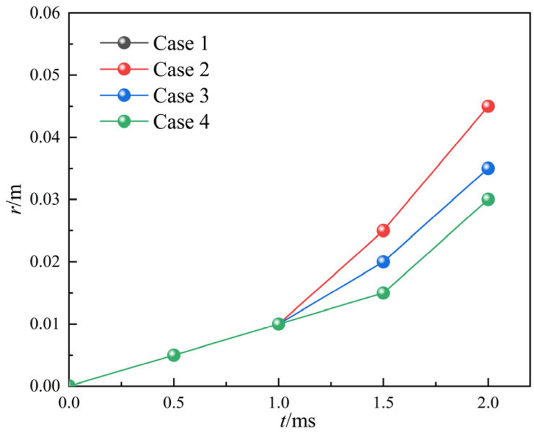

Figure 8. Radial flame transmission.

3.3. Influence of Tubular Propellant and Granular Propellant Proportion

According to the above ballistic performance analysis, the performance of the Case 2 mixture charge structure is significantly different from that of Case 1. In practice, the charging length of the tubular propellant needs to be adjusted according to tactical requirements and the length of the projectile tail. Therefore, the influence of the charging proportion of the tubular propellant and the granular propellant on ballistic performance should be investigated in detail. In this section, based on the Case 2 charging structure mentioned above, different tubular charging lengths were designed to study the influence of the mixed charging ratio. The specific calculation parameters are shown in Table 3.

Table 3. Charging scheme of different tubular and granular proportion.

Scheme	The Charging Length of Tubular/mm	The Charging Length of Granular/mm
1	300	462
2	450	312
3	600	162
4	750	12

Figure 9 shows the pressure distribution in the chamber of different tubular propellant charging lengths at 3.0 ms. The blue area represents the interface between tubular propellant and granular propellant. As shown in Figure 9, the flow field is continuously and evenly distributed in the respective distribution areas of tubular propellant and granular propellant, and the pressure demonstrates obvious discontinuity at the interface. In addition, with the increase of the tubular propellant charging area, the pressure at the bottom of the bullet rises rapidly, and the pressure in the chamber is larger.

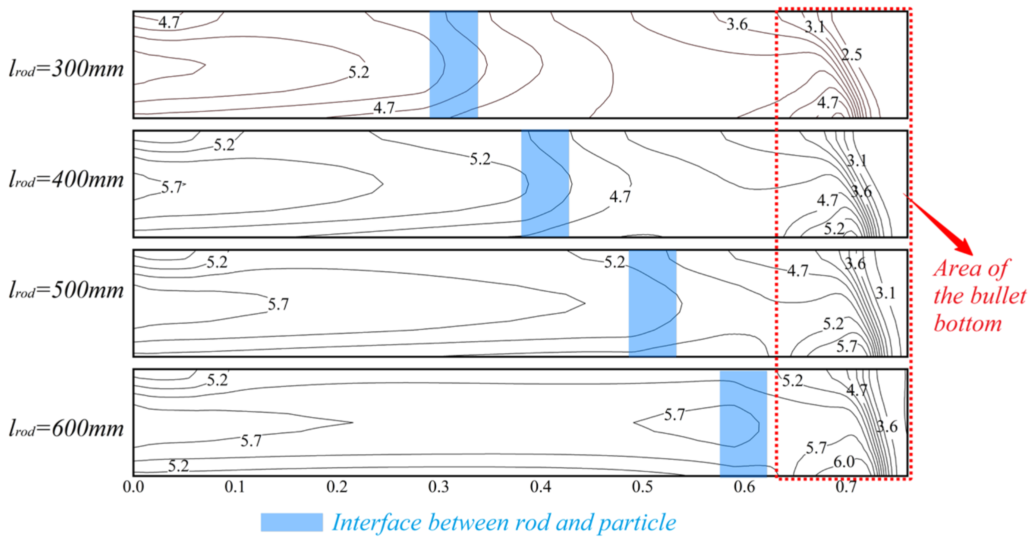

Figure 9. The pressure distribution of different tubular propellant charging lengths at 3.0 ms.

The ignition position in the chamber is shown in Figure 10. In the initial stage, the left of each charge structure is tubular propellant, so the flame propagation law is consistent. As the flame reaches the interface successively, the velocity of axial propagation is different: the longer the tube charge area, the faster the flame propagates along the axial direction. The axial propagation velocity of flame under different charge lengths was further compared, as shown in Figures 11 and 12. As can be seen from these figures, the tubular propellant can effectively increase the propagation speed of the flame. However, as the tubular length increases gradually, the increase of flame propagation speed becomes increasingly smaller.

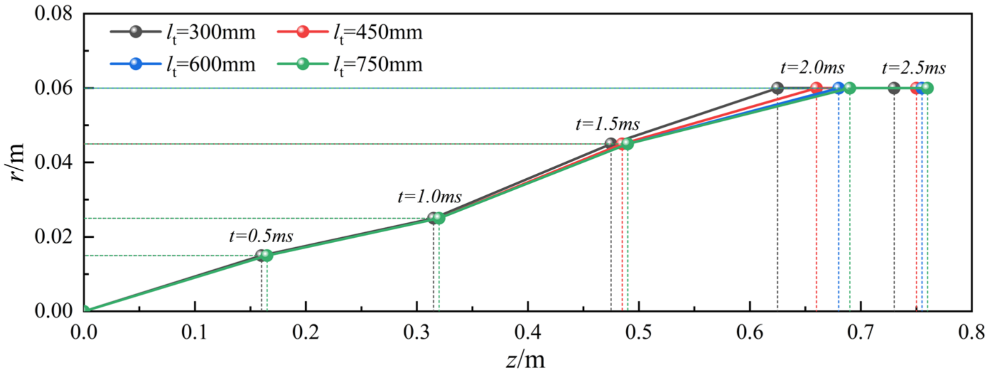

Figure 10. The ignition position of different tubular propellant charging lengths.

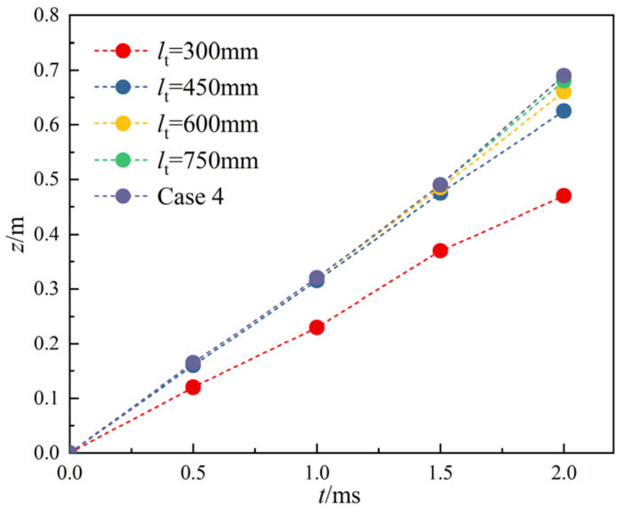

Figure 11. Axial flame transmission position.

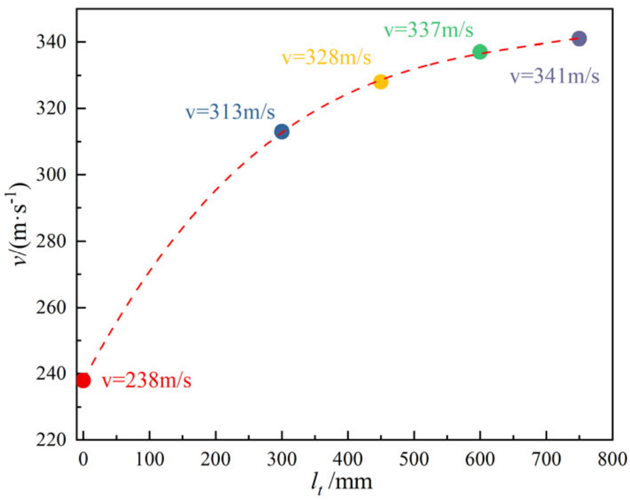

Figure 12. Axial flame transmission velocity.

Figures 13 and 14 show the variation in ballistic performance. It can be seen that changing the charging length of tubular propellant has little influence on the initial pressure rise speed. However, less tubular propellant results in higher chamber pressure and greater projectile velocity. Therefore, differing performances can be achieved by adjusting the proportion of tubular propellant.

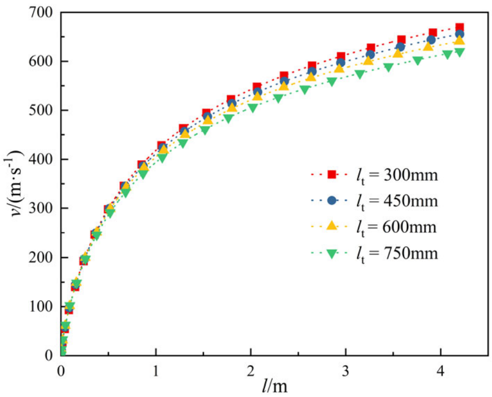

Figure 13. The velocity of different structures.

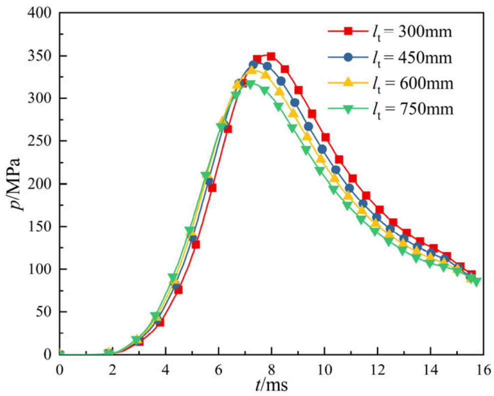

Figure 14. The pressure of different structure.

3.4. Influence of Center Charge Structure Parameters

As can be seen from previous research, the granular propellant charge pressure is high, with poor flame transmission performance and inferior ignition consistency, compared with tubular propellant charge. The central charge structure can significantly improve the fire transfer performance of granular propellant, while ballistic properties such as chamber pressure are less affected. Therefore, it is necessary to explore the flame transmission performance and ballistic performance of different center charge structure parameters, and determine the sensitivity of ballistic characteristics to structural parameters. Based on the Case 3 charge structure, the axial and radial lengths of tubular propellant are adjusted to investigate its influence on chamber pressure. The specific calculation parameters are shown in Table 4.

Table 4. Charging scheme of center charge structures.

Scheme	Radial Charging Length of Tubular/mm	Scheme	Axial Charging Length of Tubular/mm
1	5	5	300
2	10	6	450
3	15	7	600
4	20	8	750

The pressure and projectile velocity curves of central tubular propellant charge structures with the same axial length and different radial length are shown in Figure 15. As can be seen from the figure, the longer the radial length, the better the flame transmission performance and the faster the projectile velocity at the same time. However, the greater the tubular propellant charging is, the maximum chamber pressure is lowered slightly.

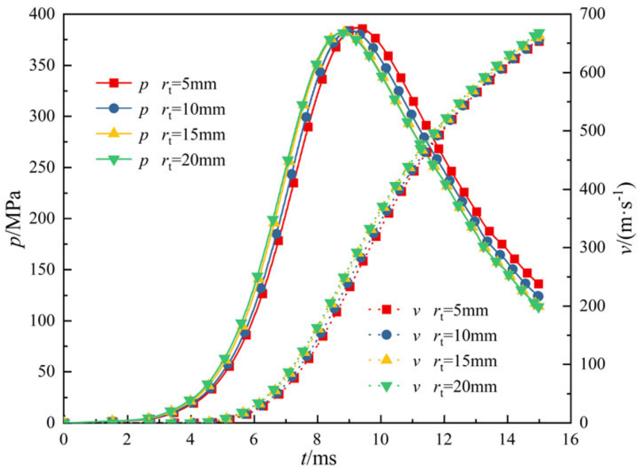

Figure 15. The ballistic curves of different radial lengths.

Figure 16 shows the pressure distribution of different radial lengths and the cloud diagram of burned percentage at 2.5 ms. The red and black areas in the figure are the relative burned percentage in the current. It can be seen that the more tubular propellant is charged, the more obvious combustion in the chamber is. The axial distribution of average pressure in the chamber is shown above the cloud diagram. It can be seen that the more tubular propellant is charged in the radial direction, the greater the pressure is in the chamber, indicating better flame transfer performance in the initial stage. On the right is the radial distribution of the average pressure in the chamber. The pressure gradually decreases from the center to the barrel boundary. At this time, the more tubular propellant, the better consistency of radial pressure is in the chamber, and the pressure is higher.

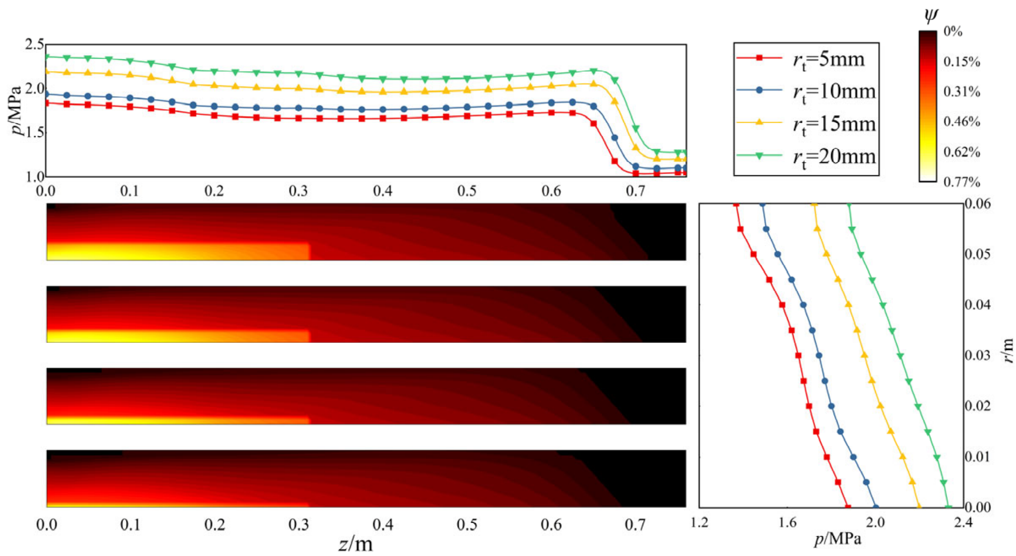

Figure 16. The pressure distribution and the cloud diagram of burned percentage of different radial lengths at 2.5 ms.

Further, increasing the axial charging length under the same radial length, and the pressure in the chamber and the velocity of the projectile are obtained, as shown in the Figure 17. As can be seen from the figure, the chamber pressure basically did not change, and with shorter axial charging length, the chamber pressure is slightly higher. Figure 18 shows the axial and radial pressure distributions of different radial charging length at 2.5 ms. There is little difference in pressure distribution at this time, which is consistent with the law of ballistic curve.

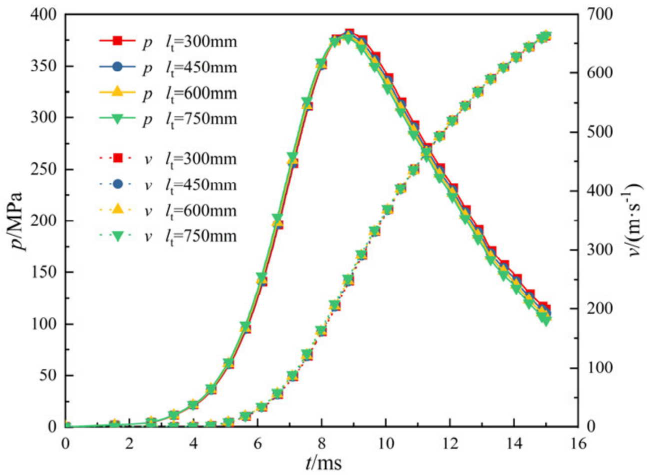

Figure 17. The ballistic curves of different axial lengths.

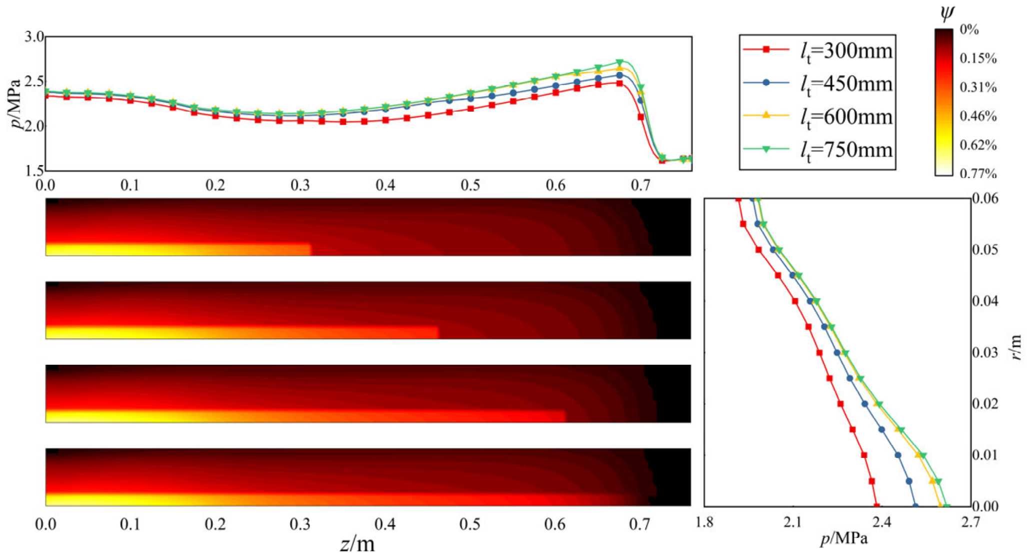

Figure 18. The pressure distribution and the cloud diagram of burned percentage of different axial lengths at 2.5 ms.

To sum up, increasing the charging length and width of tubular propellant has little influence on the flame transmission performance. In the ignition stage, the flame effect area is related to the flame propagation speed and the charge structure. Generally, the most influential part is at the bottom of the chamber, so it is most effective to conform the charge structure to the bottom of the chamber. Therefore, the chamber pressure and ignition characteristics should be considered comprehensively in a certain range when designing the appropriate charge structure.

4. Conclusions and Prospects

In this work, we establish the mathematical model of different particle types based on interior ballistics, subsequently obtaining the distribution of parameters in the chamber by the two-phase flow method, and conducting a study with different particle charge parameters to explore the sensitivity of ballistic characteristics to structural parameters. The conclusions are as follows:

(1) By comparing the four charging structures, the tubular propellant has better ignition performance than the granular propellant, and the ignition consistency can be improved by charging tubular propellant.

(2) The front and rear mixed charge structure and the center tubular propellant charge has good ignition and fire transmission performance. The flame spreading time is obviously smaller than that of the full particle charging structure, and is basically the same as that of the full tubular charging structure.
(3) The mass and ignition properties of tubular propellants are nonlinear. As the tubular length increases gradually, the increase of flame propagation speed becomes increasingly smaller. More tubular propellants are ineffective at significantly improving ignition performance, and would reduce the chamber pressure.

In the future, we will conduct more experiments to further verify the feasibility of different charge structures. Furthermore, we plan to optimize the design of charge structure, and providing more options for actual scenarios.

Author Contributions: Conceptualization, S.C. and R.T.; methodology, S.C.; software, S.C.; validation, X.L.; formal analysis, S.X.; investigation, K.J.; resources, K.J.; data curation, S.X.; writing—original draft preparation, S.C.; writing—review and editing, S.C. All authors have read and agreed to the published version of the manuscript.

Funding: This research received no external funding.

Data Availability Statement: Not applicable.

Conflicts of Interest: The authors declare no conflict of interest.

References

1. Miura, H.; Matsuo, A.; Nakamura, Y. Numerical prediction of interior ballistics performance of projectile accelerator using granular or tubular solid propellant. *Propellants Explos. Pyrotech.* **2012**, *38*, 204–213. [CrossRef]
2. El Sadek, H.; Zhang, X.; Rashad, M.; Cheng, C. Improvement of interior ballistic performance utilizing particle swarm optimization. *Math. Probl. Eng.* **2014**, *2014*, 1–10. [CrossRef]
3. Li, K.J.; Zhang, X.B. Optimization and application of interior ballistic performance with mixed-charge. *Chin. J. Explos. Propellants* **2011**, *34*, 74–79.
4. Tabrizi, A.B.; Shams, M.; Ebrahimi, R. Numerical study of gas-solid reactive flow in a cylinder. *J. Mech. Sci. Technol.* **2012**, *26*, 811–817. [CrossRef]
5. Jiang, S.Y.; Wang, H.; Lin, C.J.; Wang, J.L. Establishment and simulation of two-dimensional interior ballistics model of large caliber davis gun considering the axial movement of tubular charge clusters. *Acta Armamentarii* **2016**, *37*, 1941.
6. Jiang, S.; Wang, H. Discrete group gas-solid two-phase flow model and its simulation in the large caliber high speed davis gun. *J. Harbin Inst. Technol.* **2016**, *23*, 5.
7. Nusca, M.J.; Gough, S. Numerical Model of Multiphase Flow Applied to Solid Propellant Combustion in Gun Systems. In Proceedings of the 34th AIAA/ASME/SAE/ASEE Joint Propulsion Conference and Exhibit, Cleveland, OH, USA, 13–15 July 1998. [CrossRef]
8. Miura, H.; Matsuo, A.; Nakamura, Y. Three-Dimensional Simulation of Pressure Fluctuation in a Granular Solid Propellant Chamber within an Ignition Stage. *Propellants Explos. Pyrotech.* **2011**, *36*, 259–267. [CrossRef]
9. Wildegger-Gaissmaier, A.E.; Johnston, I.R. Ignition of a granular propellant bed. *Combust. Flame* **1996**, *106*, 219–230. [CrossRef]
10. Taylor, M.J.; Woodley, C.R. Comparison from modelling and experiment of electrothermal plasma temperature and pressure within granular propellant beds. In Proceedings of the 2004 12th Symposium on Electromagnetic Launch Technology, Snowbird, UT, USA, 25–28 May 2004.
11. Zhang, L.K.; Yu, Y.G.; Lu, X. Interior ballistics simulation of modular charge gun system using matlab. *Appl. Mech. Mater.* **2012**, *195–196*, 834–839. [CrossRef]
12. Wang, Y.W.; Zhu, W.F.; Di, J.W.; Hu, X.H. Study on the analysis method on ballistic performance of deterred propellant with large web size in large caliber artillery. *Def. Technol.* **2018**, *14*, 522–526. [CrossRef]
13. Acharya, R. Modeling and Numerical Simulation of Interior Ballistic Processes in a 120 mm Mortar System. Ph.D. Thesis, The Pennsylvania State University, State College, PA, USA, 2009.
14. Acharya, R.; Kuo, K.; Ferrara, P.; Rand, H.; Nimphius, J. Comprehensive Three Dimensional Mortar Interior Ballistics Model for 120mm Mortar System with Experimental Validation. In Proceedings of the 45th AIAA/ASME/SAE/ASEE Joint Propulsion Conference & Exhibit, Denver, CO, USA, 2–5 August 2009.
15. Schmidt, J.R.; Nusca, M.J. *Progress toward a Multidimensional Representation of Mortar Interior Ballistics*; John Wiley & Sons, Inc.: Hoboken, NJ, USA, 2009.
16. van der Hoef, M.A.; van Sint Annaland, M.; Deen, N.G.; Kuipers, J.A.M. Numerical simulation of dense gas-solid fluidized beds: A multiscale modeling strategy. *Annu. Rev. Fluid Mech.* **2008**, *40*, 47–70. [CrossRef]
17. Tsuji, Y. Multi-scale modeling of dense phase gas-particle flow. *Chem. Eng. Sci.* **2007**, *62*, 3410–3418. [CrossRef]

18. van der Hoef, M.A.; Ye, M.; van Sint Annaland, M.; Andrews, A.T.; Sundaresan, S.; Kuipers, J. Multiscale modeling of gas-fluidized beds. *Adv. Chem. Eng.* **2006**, *31*, 65–149.
19. Jaramaz, S.; Mickovic, D.; Elek, P. Two-phase flows in gun barrel: Theoretical and experimental studies. *Int. J. Multiph. Flow.* **2011**, *37*, 475–487. [CrossRef]
20. Cheng, C.; Zhang, X.B. Parallel numerical simulation on three-dimensional two-phase flow of interior ballistic trajectory. *Acta Armamentarii* **2019**, *40*, 769. (In Chinese)
21. Luo, Q.; Zhang, X.B. Numerical simulation of gas-solid two-phase reaction flow with multiple moving boundaries. *Int. J. Numer. Methods Heat Fluid Flow.* **2015**, *25*, 375–390. [CrossRef]
22. Cheng, C.; Zhang, X.B. Influence of serial and parallel structures on the two-phase flow behaviors for dual combustion chambers with a propelled body. *Powder Technol.* **2017**, *314*, 442–454. [CrossRef]
23. Nussbaum, J.; Helluy, P.; Hérard, J.M.; Carriére, A. Numerical simulations of gas-particle flows with combustion. *Flow Turbul. Combust.* **2006**, *76*, 403–417. [CrossRef]
24. Woodley, C.R.; Billett, S.; Lowe, C.; Speares, W.; Toro, E. The FHIBS internal ballistics code. In Proceedings of the 22nd International Symposium on Ballistics, Vancouver, BC, Canada, 14–18 November 2005; pp. 322–329.
25. Cheng, S.S.; Wang, H.; Xue, S.; Tao, R.Y. Application and Research of the Particle Element Model in Ignition Process of Large-Particle High-Density Charge. *Combust. Sci. Technol.* **2022**, *194*, 1850–1871. [CrossRef]
26. Cheng, C.; Zhang, X. Modeling of interior ballistic gas-solid flow using a coupled computational fluid dynamics-discrete element method. *J. Appl. Mech* **2013**, *80*, 314031–314036. [CrossRef]
27. Miura, H.; Matsuo, A.; Nakamura, Y. Interior Ballistics Simulation of Projectile Launch System Utilizing Tubular Solid Propellant. In Proceedings of the 44th AIAA/ASME/SAE/ASEE Joint Propulsion Conference & Exhibit, Hartford, CT, USA, 21–23 July 2008.
28. Cheng, C.; Zhang, X.B. Numerical investigation on the transient ignition behavior using CFD-DEM approach. *Combust. Sci. Technol.* **2014**, *186*, 1115–1137. [CrossRef]
29. Baer, M.R.; Nunziato, J.W. A two-phase mixture theory for the deflagration-to-detonation transition (ddt) in reactive granular materials. *Int. J. Multiph. Flow* **1986**, *12*, 861–889. [CrossRef]
30. Jang, J.S.; Oh, S.H.; Roh, T.S. Development of three-dimensional numerical model for combustion-flow in interior ballistics. *J. Mech. Sci. Technol.* **2016**, *30*, 1631–1637. [CrossRef]
31. Jang, J.; Oh, S.; Roh, T. Comparison of the characteristics of granular propellant movement in interior ballistics based on the interphase drag model. *J. Mech. Sci. Technol.* **2014**, *28*, 4547–4553. [CrossRef]
32. Yuan, Y.X.; Zhang, X.B. *Multiphase Hydrokinetic Foundation of High Temperature and High Pressure*; Publishing Company of Harbin Institute of Technology: Harbin, China, 2005.
33. Zhang, B.Z.; Wang, H.; Wang, S.S.; Cao, R.Y. One-dimensional two-phase flow modeling and simulation for interior ballistics of large-caliber davis gun. *J. Ballist.* **2014**, *26*, 17–21.
34. Gough, P.S. *Some Fundamental Aspects of the Digital Simulation of Convective Burning in Porous Beds*; AIAA: Orlando, FL, USA, 1977; pp. 77–855.
35. Jiang, G.; Shu, C. Efficient Implementation of Weighted ENO Schemes. *J. Comput. Phys.* **1996**, *126*, 202–228. [CrossRef]